arXiv:1601.04926v1 [cond-mat.str-el] 19 Jan 2016

Lattice vibrations of the charge-transfer salt κ-(BEDT-TTF)$_2$Cu$_2$(CN)$_3$: novel interpretation of the electrodynamic response in a spin-liquid compound

M. Dressel,[1] P. Lazić,[2] A. Pustogow,[1] E. Zhukova,[1,3,4] B. Gorshunov,[1,3,4]
J. A. Schlueter,[5] O. Milat,[6] B. Gumhalter,[6] and S. Tomić[6]

[1] *1. Physikalisches Institut, Universität Stuttgart, Pfaffenwaldring 57, 70550 Stuttgart Germany*
[2] *Rudjer Bošković Institute, Bijenička cesta 54, HR-10000 Zagreb, Croatia*
[3] *A.M. Prokhorov General Physics Institute, Russian Academy of Sciences, 119991 Moscow, Russia*
[4] *Moscow Institute of Physics and Technology (State University), 141700, Dolgoprudny, Moscow Region, Russia*
[5] *Material Science Division, Argonne National Laboratory - Argonne, Illinois 60439-4831, U.S.A.*
[6] *Institut za fiziku, P.O.Box 304, HR-10001 Zagreb, Croatia*

(Dated: January 20, 2016)

The dimer Mott insulator κ-(BEDT-TTF)$_2$Cu$_2$(CN)$_3$ exhibits unusual electrodynamic properties. Numerical investigations of the electronic ground state and the molecular and lattice vibrations reveal the importance of the $Cu_2(CN)_3^-$ anion network coupled to the BEDT-TTF molecules: The threefold cyanide coordination of copper and linkage isomerism in the anion structure cause a loss of symmetry, frustration, disorder, and domain formation. Our findings consistently explain the temperature and polarization-dependent THz and infrared measurements, reinforce the understanding of dielectric properties and have important implications for the quantum spin-liquid state, which should be treated beyond two-dimensional, purely electronic models.

PACS numbers: 71.45.-d, 71.30.+h, 75.10.Kt, 78.55.Kz 63.20.-e

In the field of quasi-two-dimensional strongly correlated electron systems, the κ-salts of the BEDT-TTF family have attracted considerable interest [1] because their triangular arrangement of the dimers is close to geometrical frustration leading to the first realization of spin-liquid behavior in κ-(BEDT-TTF)$_2$Cu$_2$(CN)$_3$ [2]. The antiferromagnetic exchange coupling among the dimers is rather strong ($J \approx 250$ K), however, neither the magnetic order nor structural distortions have been detected down to lowest temperatures. Despite enormous theoretical and experimental efforts, the nature of this phase is still inconclusive and the question of a possible gap in the spin excitations remains open [3–6]. From the residual spin susceptibility and the power-law temperature dependence of the NMR spin-lattice relaxation rate, low-lying spin excitations are concluded, while their contribution to the optical conductivity is still under discussion [7–9].

Interacting spins on a triangular lattice cannot order in a simple antiferromagnetic ground state, quantum fluctuations prevent a stable spin-liquid phase in the presence of finite hopping t and electronic repulsion U. More advanced microscopic models have been put forward to explain the properties of κ-BEDT-TTF salts [10–13] based on the presence of charge dipoles on the dimers which couple to spin degrees of freedom and thereby prevent ordering. While the electronic order has been proven in related compounds [14] in which the intra-dimer Coulomb repulsion U is reduced with respect to inter-site interaction V, the ratio V/t is of minor relevance in the case of κ-(BEDT-TTF)$_2$Cu$_2$(CN)$_3$, called κ-CN (Fig. 1). The anomalous dielectric response observed in the kHz and MHz range below 60 K [20, 21] evidences some unexpected charge excitations in the spin-liquid state which must be explained satisfactorily. Recently, time-domain optical measurements rendered a rather broad absorption band around 1 THz that develops below $T \approx 80$ K. Itoh *et al.* [22] attributed it to collective excitation of intra-dimer electric dipoles. However, NMR, Raman and infrared spectroscopies rule out any sizable charge imbalance all the way down to low temperatures [24–26].

In order to shed light on the excitation properties in the quantum spin-liquid state in general, and the prototypical dimer system κ-CN in particular, we have performed broad-band optical investigations with the emphasis on

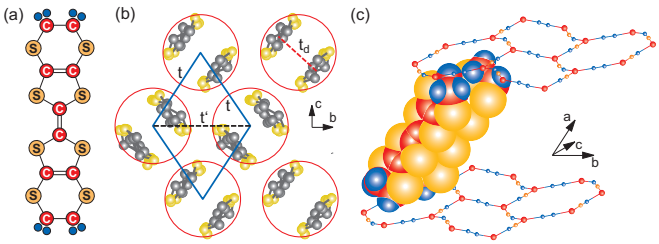

Figure 1: (Color online) (a) Sketch of the bis-(ethylenedithio)-tetrathiafulvalene molecule, called BEDT-TTF. (b) For κ-(BEDT-TTF)$_2$Cu$_2$(CN)$_3$ they are arranged in dimers, which constitute an anisotropic triangular lattice within the *bc* conduction layers. (c) These BEDT-TTF layers are sandwiched along the *a*-axis by insulating anion sheets. The polymerized $Cu_2(CN)_3^-$ form interconnected elongated hexagons with the terminal ethylene groups of a BEDT-TTF dimer fitting into the opening. The ratio of the inter-dimer transfer integrals is close to unity: $t'/t \approx 0.83$ [15, 16]; the intra-dimer transfer integral $t_d \approx 0.2$ eV [17, 18]. With $U \approx 2t_d$ [19], one obtains at ambient conditions $U/t = 7.3$; a slight variation of U and orbital overlap t causes magnetic order, on the one hand, and superconductivity, on the other hand.

the THz and far-infrared spectral range complemented by the first extensive DFT calculations of the electronic structure and vibrational properties. Thereby we bridge the gap between microscopic models and macroscopic observations. We find that in κ-CN not only the triangular arrangement of the dimers is important, but also the anions exhibit intrinsic frustration and disorder due to polar cyanide links between the three-fold bound Cu ions. Specifically, we make clear that the low-energy modes in the THz range are lattice vibrations rather than collective dimer excitations: the dominant motion of the $Cu_2(CN)_3^-$ anions is strongly coupled to the BEDT-TTF dimers.

The in- and out-of-plane infrared reflectivity of κ-CN single crystals was measured with 1 cm^{-1} spectral resolution using several Fourier-transform spectrometers equipped with proper polarizers in order to probe the electrodynamic response in different directions and at the temperatures 300 K $> T >$ 5 K. The optical conductivity is obtained by standard Kramers-Kronig analysis; for further detail see Refs. [9, 26]. At very low frequencies $\nu < 45$ $cm^{-1} \hat{=} 1.5$ THz, we were able to perform transmission experiments on a very large single crystal (2×4 mm^2) as for $T \leq 100$ K the absorption becomes small enough. Employing a coherent source THz Mach-Zehnder interferometer [S2] both the amplitude and phase change can be measured independently with high spectral resolution and accuracy. The optical conductivity is directly calculated by Fresnel's equations and plotted in Fig. 2 for different polarizations and temperatures as indicated. The corresponding permittivity is shown in Fig. S1 of the Supplemental Materials [27].

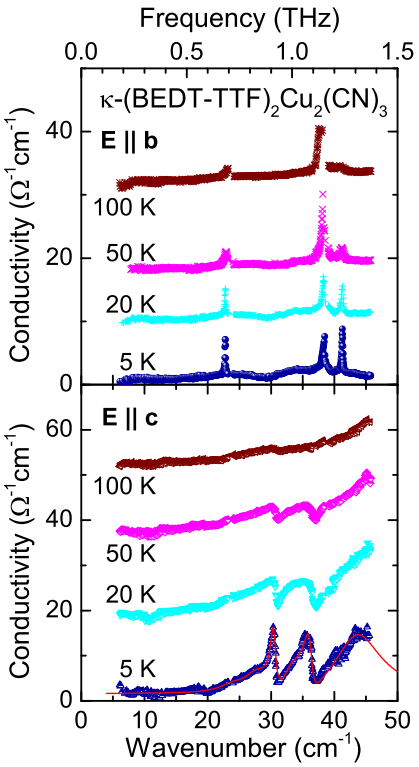

Figure 2: (Color online) THz-spectra of the optical conductivity of κ-$(BEDT\text{-}TTF)_2Cu_2(CN)_3$ measured at different temperatures for both polarizations using a coherent-source Mach-Zehnder interferometer. The data are shifted with respect to each other for clarity reasons. The red line corresponds to the fit of the data.

For $E \parallel b$ we observe a phonon-like doublet around 40 cm^{-1} and another mode around 23 cm^{-1}. As expected for a vibrational feature, the latter one continuously narrows and becomes more pronounced as the crystal is cooled. Interestingly, when the temperature is reduced below 60 K a rather sharp peak at 41.3 cm^{-1} grows drastically at the expense of the 38.5 cm^{-1} mode. Also for $E \parallel c$ between 30 and 40 cm^{-1} actually two distinct features become very prominent at low temperatures. In accord with Ref. [22], the peaks grow for $T < 60$ K; they have a rather unusual sawtooth shape, that can only be fitted satisfactorily by two Fano functions and a Lorentzian on top of a power-law background [9].

In order to assign and finally understand the observed vibrational features, we have carried out first-principles calculations of the electronic structure in the framework of the density functional theory (DFT) as implemented in the VASP code using the projector augmented-wave method [27–29]. The structural data obtained by x-ray investigations at $T = 100$ K are solved in $P2_1$ symmetry and reduced to $P1$ which turns out to be the relaxed structure of lowest energy. The obtained electronic band structure of the κ-CN system is in accord with previous calculations [15, 16] and plotted in Fig. S3; two antibonding bands of BEDT-TTF molecules cross the Fermi level and the bonding bands lie well below it. The overall cation-derived character of kappa-CN band structure around the Fermi level is also confirmed by the rigid band shift of molecular subsystem alone that is induced by the charge transfer of nearly two electrons [27]. Despite the cation-band character around the Fermi level, the anion layer turns out to be crucial for the full understanding of this charge transfer salt.

Hence we now turn to the $Cu_2(CN)_3^-$ network; in Fig. 3 we can identify two segregated chains mainly directed along the b-axis. Each Cu is linked to the three neighboring Cu ions by cyanide groups; in one of them the CN are arranged in positive direction, here labeled as b_1 and b_2, while the groups b_3 and b_4 point in the negative direction. Inverting one CN costs 174 meV; if all four groups are oriented parallel, the energy of the lattice is enhanced by 240 meV. This falls into the energy range of few hundred meV known for a cyanide flip in the case of linkage isomerism [31–33].

Even more interesting are the two bridging links c_1 and c_2 for which the cyano groups are directed dominantly along the c-axis. Commonly the structure is solved within the $P2_1/c$ symmetry implying that due to

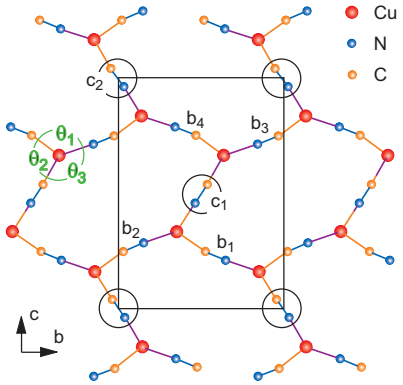

Figure 3: (Color online) Relaxed structure of the $Cu_2(CN)_3^-$ anion layer in the bc plane of κ-(BEDT-TTF)$_2$Cu$_2$(CN)$_3$ as obtained by the DFT calculations. The unit cell contains two formula units ($Z = 2$) with two distinct configurations of Cu ions. When the positions of C and N in the encircled links are specified, the symmetry is reduced to P1. For the sake of simplicity, only the inequivalency between the bridging c_1 and c_2 is shown. The coordination at the Cu site ($\theta_1 = 118.7°$, $\theta_2 = 102.3°$, $\theta_3 = 138.8°$) is closer to the ideal 120° than for other polyanions [37]. This constellation is prone to frustration, disorder and domain formation.

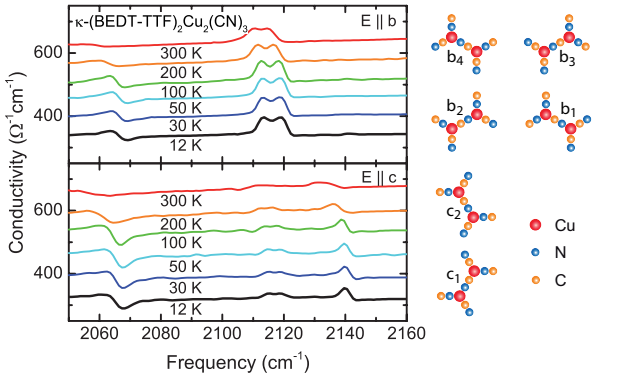

Figure 4: (Color online) Mid-infrared conductivity of κ-(BEDT-TTF)$_2$Cu$_2$(CN)$_3$ recorded for the polarization $E \parallel b$ and $E \parallel c$ at different temperatures. The CN stretching modes are seen between 2115 and 2140 cm^{-1}. On the right the different cyanide arrangements in the lowest energy state are sketched. For $E \parallel c$ the two arrangements c_1 and c_2 are degenerate in energy.

the linkage isomerization they sit at inversion centers, i.e. the orientation is stochastic [34]. Recent x-ray scattering studies [21] already suggested that the lower symmetry group may be more relevant; this is now confirmed by the present calculations as well as by the targeted structural studies [35]: the crystallographic structure of κ-CN is best characterized by the low symmetry group $P1$. The energy minimum is reached for both c-cyanides aligned in the same direction as pictured in Fig. 3. However, the energy difference relative to the situations of reversed (parallel as well as antiparallel) cyanides is only 10 to 15 meV, i.e. one order of magnitude less than for the inversion of cyanides in the b-chains. From the Cu-ion point of view, the linkage isomerism causes frustration as they may be coordinated to two C and one N atoms, or to one C and two N, paving the way for intrinsic disorder. The consequence is a local rearrangement of the lattice. Naturally, the domains of local order of one or the other preferential direction will form. Coupling via hydrogen bonds to the ethylene groups extends the distortions of the anion network onto the BEDT-TTF layers. This fact might explain the relaxor-like low-frequency dielectric response observed previously [20, 21].

The phonon modes are calculated with the PHONOPY code [36] using the DFT-derived force constants [28]. Among the 360 vibrations obtained in the spectral range up to approximately 3000 cm^{-1} $\hat{=}$ 90 THz [27] let us consider first the stretching motion of the anions where the cyanides move between the heavy Cu ions basically without affecting the other constituents. The 2139 cm^{-1} feature observed for $E \parallel c$ (Fig. 4) can be assigned to vibrations of the c_1 and c_2 groups calculated to appear at $\nu_{327} = 2131.8$ cm^{-1} and $\nu_{328} = 2136.0$ cm^{-1}, for the out-of-phase and in-phase motion, respectively. The four b-type CN groups are expected to oscillate at 2089.9, 2095.1, 2101.6, and 2106.8 cm^{-1} and can be associated with the double structure seen in Fig. 4 at 2113 and 2118 cm^{-1} for $T = 100$ K, as an example. Other cyanide modes are identified at around 320 and 500 cm^{-1} (cf. Fig. S2). The important result from our infrared data is a rather strong anisotropy of the cyanide vibrational features. The bridging $c_1$and c_2 groups possess larger force constants than the four b-type CN groups. This may be due to shorter and more rigid Cu-CN-Cu bonds, implying steeper potentials for the bridging than for the four b-type CN groups. Such a contribution prevails over the standard charge-density term. Namely, our calculations of the cation-anion interaction-induced charge distribution demonstrate that at the cyanide sites the electron density is enhanced compared to the bare one without the BEDT-TTF molecules; this effect is much stronger along the b-chains than along the bridging c-axis (Figs. S4 and S5).

More remarkable, however, are the pronounced modes in the THz range, which involve bending and twisting motions of larger entities, or of the anions as a whole. Our calculations evidence that these low-energy features contain the anions as well as the BEDT-TTF cations, i.e. they are lattice phonons rather than molecular vibrations [38–40]. The cyano groups in κ-CN possess static dipole moments and interact with BEDT-TTF molecules; these polar links are found to be larger for the four b-type cyanides than for the bridging c_1 and c_2-bonds (Fig. S5).

The computed frequencies of the long-wavelength vibrations are in good agreement with the measured optically excited phonons in the THz range (see Fig. 2), as

Table I: Vibrational modes of κ-(BEDT-TTF)$_2$Cu$_2$(CN)$_3$ in the THz range. The observed features of Fig. 2 are compared to modes obtained by *ab-initio* phonon calculations based on density-functional-theory. A complete list and 3D motion pictures are given in the Supplemental Materials [27].

Mode No.	$E \parallel b$		$E \parallel c$	
	calc. (cm^{-1})	exp. (cm^{-1})	calc (cm^{-1})	exp. (cm^{-1})
4	24.3	22.7		
5			33.3	31.2
8			37.8	37.0
9	38.2	38.4		
11	40.5	41.3		

demonstrated in Tab. I. For $E \parallel b$ two modes are calculated to appear at $\nu_9 = 38.2$ and at $\nu_{11} = 40.5$ cm^{-1}, which involve coupled cation-anion motion: bending of the complete dimer followed by shear and waving motion of the anion layer. The outer rings of BEDT-TTF are particularly affected by the higher-frequency excitation. The corresponding features for $E \parallel c$ are related to twist motions of the BEDT-TTF dimer with a strong involvement of the ethylene groups; again the dimer motion is coupled to shear motion of the anion layer.

The phonon lineshape for the two polarizations shown in Fig. 2 is notably different: in the case of $E \parallel b$ they exhibit a simple Lorentzian structure, whereas for $E \parallel c$ these are asymmetric Fano-like lineshapes. In the first case the photons couple directly to the optical phonons [41]; the effect becomes even stronger as the charge density in the anion layers is enhanced along the b-direction by the cation-anion interaction. For the c-polarization, additional resonant interactions with a continuum of excitations must be invoked to cause Fano-interference effects. Spinons have been suggested as candidates for these low-energy excitations responsible for the concomitant increase of the background THz conductivity [7, 8]. However, the experimentally observed exponents differ by more than a factor of two from the theoretically predicted ones [9]. Alternatively, the excitation continuum in the THz range may be associated with intraband electronic excitations, i.e. the creation of soft electron-hole pairs across the Fermi level in the ΓZ and ΓY directions of the first Brillouin zone (cf. Fig. S3). However, photons cannot induce these electronic transitions directly because of momentum conservation. The mechanism of resonant excitation of electron-hole pairs by optical phonons [42] requires that one photon simultaneously creates an intraband electron-hole pair and a sub-THz phonon with opposite momentum in the end-vertices of the optical response function. Such interactions are discussed in detail in Ref. [41]. Together with the selection rules favoring the photon coupling to intraband excitations for $E \parallel c$, this excitation scenario can explain the different lineshapes seen in Fig. 2. The intensity of the phonon peaks diminishes as the temperature increases. This may indicate that the phase space for the excitation of soft electron-hole pairs across the Fermi level becomes blurred; the smearing of sharp phonon features in electron-phonon interactions may also be caused by enhanced anharmonic couplings.

Our findings demonstrate that the strong THz features cannot be caused by collective excitations of the electric dipoles fluctuating within the dimers as suggested in Ref. [22]. Rather, they are due to the coupled BEDT-TTF-anion vibrations involving the entire lattice. The relation to the low-frequency dielectric response that occurs below $T \approx 60$ K [20] is certainly not by microscopic dipoles within the BEDT-TTF dimers which have been ruled out by vibrational spectroscopy [26]. Instead we suggest that the relaxor ferroelectric mode is related to the charge inhomogeneities caused by frustration and disorder in the triangular pattern of the $Cu_2(CN)_3^-$ anion layers originating in the isomorphism in the cyanides which carry a rather strong dipole moment. The coupling of organic molecules to the anion layers via the ethylene groups imposes large-scale charge inhomogeneities and domain walls onto the BEDT-TTF layer. This is in fact what is observed in the macroscopic dielectric response [20, 21]. Our conclusions are in line with calculations [43] that show the essential role of anions at the charge ordering transition of α-(BEDT-TTF)$_2$I$_3$. In the present case, however, no static charge-order develops but two highly-frustrated subsystems interact.

Our comprehensive experimental and numerical investigations of κ-(BEDT-TTF)$_2$Cu$_2$(CN)$_3$ combine optical measurements with the electronic structure and vibrational dynamics calculations. They enable us to understand how the intrinsic $Cu_2(CN)_3^-$ anion structure causes frustration, disorder, loss of symmetry and domain formation. Thereby we can consistently explain the absence of charge disproportionation on the BEDT-TTF dimers, the signatures of cyanide vibrations, the pronounced anisotropic phonon modes in THz regime, and the relaxor-like dielectric response occurring below $T = 60$ K. The intrinsic domain structure and frustration within the coupled BEDT-TTF and $Cu_2(CN)_3^-$ anion system are the origin of the electrodynamic response. This immediately implies that the interaction with the anion layer and the structure of $Cu_2(CN)_3^-$ network is crucial for understanding the quantum spin-liquid state in κ-(BEDT-TTF)$_2$Cu$_2$(CN)$_3$. Further experimental and theoretical studies will clarify whether this new level of complexity provides the missing link to stabilize this unusual ground state.

We would like to thank P. Foury, V. Ilakovac, J.-P. Pouget and G. Saito for many enlightening discussions. We acknowledge financial support by the Deutsche Forschungsgemeinschaft (DFG), Deutscher Akademischer Austauschdienst (DAAD), the Russian Ministry of Education and Science (Program 5 top 100) and the

Croatian Science Foundation project IP-2013-11-1011.

[1] K. Kanoda and R. Kato, Annu. Rev. Condens. Matter Phys. **2**, 167 (2011); B. J. Powell and R. H McKenzie, Rep. Prog. Phys. **74**, 056501 (2011).

[2] Y. Shimizu, K. Miyagawa, K. Kanoda, M. Maesato, and G. Saito, Phys. Rev. Lett. **91**, 107001 (2003): Y. Kurosaki, Y. Shimizu, K. Miyagawa, K. Kanoda, G. Saito, Phys. Rev. Lett. **95**, 177001 (2005).

[3] S. Yamashita, Y. Nakazawa, M. Oguni, Y. Oshima, H. Jojiri, K. Miyagawa, and K. Kanoda, Nature Phys. **4**, 459 (2008).

[4] M. Yamashita, N. Nakata, Y. Kasahara, T. Sasaki, N. Yoneyama, N. Kobayashi, S. Fujimoto, T. Shibauchi, and Y. Matsuda, Nature Phys. **5**, 44 (2009).

[5] R. Kaneko, S. Morita, and M. Imada, J. Phys. Soc. Jpn. **83**, 093707 (2014).

[6] P. A. Lee, Science **321**, 1306 (2008); L. Balents, Nature **464**, 199 (2010).

[7] T.-K. Ng and P. A. Lee, Phys. Rev. Lett. **99**, 156402 (2007).

[8] I. Kezsmárki, Y. Shimizu, G. Mihaly, Y. Tokura, K. Kanoda, and G. Saito, Phys. Rev. B **74**, 201101 (2006).

[9] S. Elsässer, D. Wu, M. Dressel, and J. A. Schlueter, Phys. Rev. B **86**, 155150 (2012); A. Pustogow, E. Zhukova, B. Gorshunov, M. Pinterić, S. Tomić, J. A. Schlueter, and M. Dressel, arXiv:1412.4581.

[10] C. Hotta, J. Phys. Soc. Japan **72** 840 (2003); Phys. Rev. B **82**, 241104 (2010); Crystals **2**, 1155 (2012).

[11] M. Naka and S. Ishihara, J. Phys. Soc. Jpn. **79**, 063707 (2010); J. Phys. Soc. Jpn. **82**, 023701 (2013).

[12] H. Li, R. T. Clay, and S. Mazumdar, J. Phys.: Condens. Matter **22**, 272201 (2010); S. Dayal, R. Clay, H. Li, and S. Mazumdar, Phys. Rev. B **83** 245106 (2011); R. T. Clay, S. Dayal, H. Li, and S. Mazumdar, phys. stat sol. (b) **249**, 991 (2012).

[13] H. Gomi, M. Ikenaga, Y. Hiragi, D. Segawa, A. Takahashi, T.J. Inagaki, and M. Aihara, Phys. Rev. B **87**, 195126 (2013).

[14] N. Drichko, R. Beyer, E. Rose, M. Dressel, J. A. Schlueter, S. A. Turunova, E. I. Zhilyaeva, and R. N. Lyubovskaya, Phys. Rev. B **89**, 075133 (2014); S. Yasin, E. Rose, M. Dumm, N. Drichko, M. Dressel, J. A. Schlueter, E. I. Zhilyaeva, S. A. Turunova, and R. N. Lyubovskaya, Physics B **407**, 1689 (2012).

[15] K. Nakamura, Y. Yoshimoto, T. Kosugi, R. Arita, and M. Imada, J. Phys. Soc. Jpn. **78**, 083710 (2009).

[16] H. C. Kandpal, I. Opahle, Y.-Z. Zhang, H. O. Jeschke, and R. Valentí, Phys. Rev. Lett. **103**, 067004 (2009); H. O. Jeschke, M. de Souza, R. Valentí, R. S. Manna, M. Lang, and J. A. Schlueter, Phys. Rev. B **85**, 035125 (2012); J. Ferber, K. Foyevtsova, H. O. Jeschke, and R. Valentí, Phys. Rev. B **89**, 205106 (2014).

[17] K. Oshima, T. Mori, H. Inokuchi, H. Urayama, H. Yamochi, and G. Saito, Phys. Rev. B **38**, 938 (1988).

[18] T. Komatsu, N. Matsukawa, T. Inoue, and G. Saito, J. Phys. Soc. Jpn. **65**, 1340 (1996).

[19] R.H. McKenzie, Comments Cond. Mat. **18**, 309 (1998).

[20] M. Abdel-Jawad, I. Terasaki, T. Sasaki, N. Yoneyama, N. Kobayashi, Y. Uesu, and C. Hotta, Phys. Rev. B **82**, 125119 (2010).

[21] M. Pinterić, M. Čulo, O. Milat, M. Basletić, B. Korin-Hamzić, E. Tafra, A. Hamzić, T. Ivek, T. Peterseim, K. Miyagawa, K. Kanoda, J. A. Schlueter, M. Dressel, and S. Tomić, Phys. Rev. B **90**, 195139 (2014); M. Pinterić, T. Ivek, M. Čulo, O. Milat, M .Basletić, B. Korin-Hamzić, E. Tafra, A. Hamzić, M. Dressel, and S. Tomić, Physica B **460**, 202 (2015).

[22] K. Itoh, H. Itoh, M. Naka, S. Saito, I. Hosako, N. Yoneyama, S. Ishihara, T. Sasaki, and S. Iwai, Phys. Rev. Lett. **110**, 106401 (2013).

[23] B. P. Gorshunov, A. Volkov, I. E. Spektor, A. S. Prokhorov, A. A. Mukhin, M. Dressel, S. Uchida, and A. Loidl, Int. J. Infrared Millimeter Waves **26**, 1217 (2005).

[24] Y. Shimizu, K. Miyagawa, K. Kanoda, M. Maesato, and G. Saito, Phys. Rev. B **73**, 140407 (2006); K. Kanoda (private communication).

[25] T. Yamamoto, K. Matsushita, Y. Nakazawa, K. Yakushi, M. Tamura, and R. Kato (unpublished).

[26] K. Sedlmeier, S. Elsässer, D. Neubauer, R. Beyer, D. Wu, T. Ivek, S. Tomić, J. A. Schlueter, and M. Dressel, Phys. Rev. B **86**, 245103 (2012).

[27] See Supplemental Material at http://link.aps.org./ supplemental/ for more details, a complete list and 3D motion pictures of the calculated vibrational frequencies.

[28] G. Kresse and J. Hafner, Phys. Rev. B **47**, 558 (1993) and **48**, 13115 (1993); G. Kresse and J. Furthmüller, Comput. Mat. Sci. **6**, 15 (1996); G. Kresse and J. Furthmüller, Phys. Rev. B **54**, 11169 (1996).

[29] P. E. Blöchl, Phys. Rev. B **50**, 17953 (1994).

[30] G. Kresse and D. Joubert, Phys. Rev. B **59**, 1758 (1999)

[31] C. A. Bignozzi, C. Chiorboli, M. T. Indelli, F. Scandola, V. Bertolasi, and G. Cilli, J. Chem. Soc. Dalton Trans. **1994**, 2391 (1994).

[32] A. Shatruk, A. Dragulescu-Andrasi, K. E. Chambers, S. A. Stoian, E. L. Bominaar, C. Achim and K. R. Dunbar, J. Am. Chem. Soc. **129**, 6104 (2007).

[33] M. F. Dumont, O. N. Risset, E. S. Knowles, T. Yamamoto, D. M. Pajerowski, M. W. Meisel, and D. R. Talham, Inorg. Chem. **52**, 4494 (2013).

[34] U. Geiser, H. H. Wang, K. D. Carlson, J. M. Williams, H. A. Charlier, J. E. Heindl, G. A. Yaconi, B. J. Love, M. W. Lathrop, J. E. Schirber, D. L. Overmyer, J. Q. Ren, and M. -H. Whangbo, Inorg. Chem. **30**, 2586 (1991).

[35] P. Foury-Leylekian et al., to be submitted (2015)

[36] A. Togo, F. Oba, and I. Tanaka, Phys. Rev. B **78**, 134106 (2008).

[37] T. Hiramatsu, Y. Yoshida, G. Saito, A. Otsuka, and H. Yamochi, J. Mater. Chem. C **3**, 1378 (2015).

[38] M. Dressel, J.E. Eldridge, J. M. Williams, and H. H. Wang, Physica C **203**, 247 (1992).

[39] A. Girlando, M. Masino, G. Visentini, R. G. Della Valle, A. Brillante, and E. Venuti, Phys. Rev. B **62**, 14476 (2000).

[40] M. Dressel, M. Dumm, T. Knoblauch, and M. Masino, Crystals **2**, 528 (2012).

[41] A.S. Davydov, *Solid State Theory* (Nauka, Moscow, 1976) (in Russian), Ch. III; G.D. Mahan, *Many Particle Physics* (Plenum, New York and London, 1981), Chs. 4 and 8.1.

[42] E. Cappelluti, L. Benfatto, and A.B. Kuzmenko, Phys. Rev B **82**, 041402 (2010).

[43] P. Alemany, J-P. Pouget and E. Canadell, Phys. Rev B **85**, 195118 (2012)

Supplemental Material

THZ RESPONSE

Using a Mach-Zehnder interferometer in the frequency domain allows us to measure independently the optical transmission and phase change in the THz frequency range from 6 to 46 cm^{-1} with an extremely high spectral resolution of 0.05 cm^{-1}. The frequency dependent conductivity $\sigma(\nu)$ and permittivity $\epsilon(\nu)$ are then calculated by using Fresnel's equations for each frequency [S1, S2] without assuming any model. In Fig. S5 the optical conductivity (reproduced from Fig. 2 of the main text) is complemented by the permittivity for both polarizations $E \parallel b$ and $E \parallel c$ at different temperatures. It is interesting to note the pronounced anisotropy in the dielectric constant: for the lowest frequency we find $\epsilon_b \approx 30$ while $\epsilon_c \approx 50$ in the c-direction is more or less independent on temperature. This observation is in accord with the anisotropic response in the conductivity.

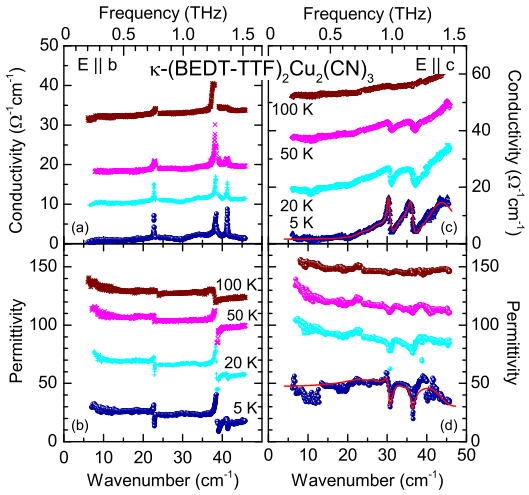

Figure S5: Frequency dependence of (a,c) the optical conductivity and (b,c) the dielectric constant of κ-(BEDT-TTF)$_2$Cu$_2$(CN)$_3$ measured in the THz range at different temperatures for both polarizations (a,b) $E \parallel b$ and (c,d) $E \parallel c$ using a coherent source Mach-Zehnder interferometer. The data are shifted with respect to each other for clarity reasons. The red line corresponds to the fit of the data by two Fano functions and a Lorentzian on top of a power-law background.

INFRARED VIBRATIONS

Besides the THz lattice vibrations displayed in Fig. S5 and the typical molecular vibrations in fingerprint mid-infrared regime, plotted in Fig. 4 of the main paper, we do also observe characteristic features of the cyanide vibrations in the far-infrared spectral range, as displayed in Fig. S6. These features are associated with vibrational motions of BEDT-TTF molecules with a strong participation of the ethylene groups. The mode seen at 487 cm^{-1} for $E \parallel c$ is related to a vibrational motion of the cyanide groups with respect to the copper ions. For $E \parallel b$ two separated features are observed at 473 and 486 cm^{-1}, which are related mainly to the b_2 and b_4 bonds in one case and b_3, b_4 and b_1, b_2 in the other case.

It is interesting to note that for both polarizations the 455 cm^{-1} modes shift to higher frequencies when the temperature is reduced from $T = 300$ K to 50 K, but seem to red-shift slightly at lower temperatures. The 487 cm^{-1} features do not exhibit this hardening at elevated temperatures. More detailed studies with higher resolution are in progress.

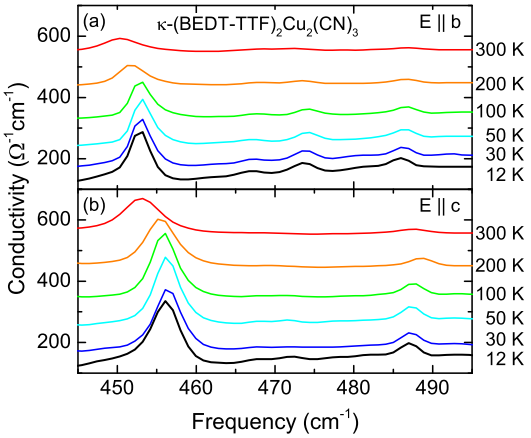

Figure S6: Far-infrared conductivity spectra of κ-(BEDT--TTF)$_2$Cu$_2$(CN)$_3$ recorded for the polarization $E \parallel b$ and $E \parallel c$ at different temperatures as indicated.

COMPUTATIONAL DETAILS, ELECTRONIC STRUCTURE AND VIBRATIONAL FREQUENCIES

We have employed the self-consistently implemented van der Waals density functional (vdW-DF) [S3, S4, S5] for correlation with optB88 for exchange [S6]. The expansion in plane waves was done with a cutoff energy of 700 eV, the Brillouin zone was sampled by $1 \times 2 \times 2$ Monkhorst-Pack choice of k-points [S7]. We relaxed the full unit-cell shape/volume and the atomic positions til the forces on the atoms dropped below 1 meV/Å.

The electronic band structure of the whole κ-(BEDT-TTF)$_2$Cu$_2$(CN)$_3$ system is plotted by black lines in Fig. S7; two antibonding bands of BEDT-TTF molecules cross the Fermi level and the bonding bands lie well

below it. Most interestingly, the generic cation bands (blue lines) calculated solely for the molecular subsystem exhibit the dimerization gap of approximately 0.5 eV, confirming the estimates from optical measurements [S8, S9, S10]. Hence, the overall cation-derived character of κ-(BEDT-TTF)$_2$Cu$_2$(CN)$_3$ band structure around the Fermi level is evident. Even though the band structure shape of the whole system around the Fermi level is fully determined by the molecular subsystem (as confirmed by the rigid band shift) - the position of the Fermi level alone is determined by the charge transfer (doping) between the anion and cation subsystems - showing strong coupling between the two. The importance of their interaction (through molecular band doping - i.e. charge transfer) is manifested through the system properties such as energy differences of the various structural configurations and phonon frequencies.

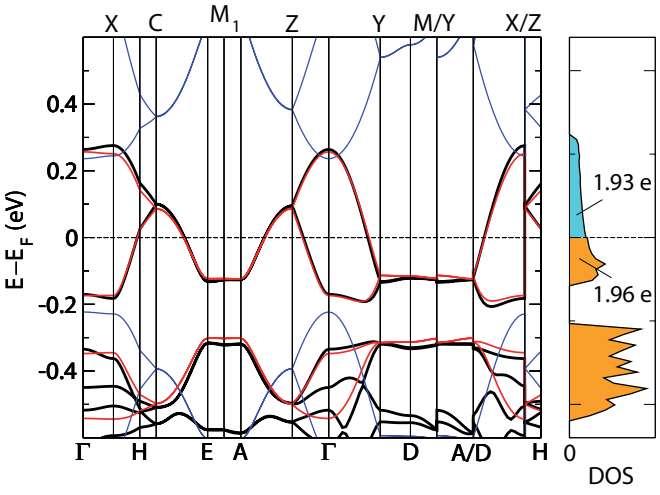

Figure S7: Band structure of κ-(BEDT-TTF)$_2$Cu$_2$(CN)$_3$ (black) plotted along the high-symmetry directions. The segments ΓZ and ΓY in the first Brillouin zone correspond to the c- and b-directions, respectively. If only the molecular subsystem is considered, the generic cation bands (blue) are obtained. Shifting them by 480 meV (red) results in an almost perfect coincidence with the complete band structure of κ-(BEDT-TTF)$_2$Cu$_2$(CN)$_3$, pointing to the overall cation-derived character around the Fermi level. The occupation of the corresponding density of states (right panel), indicates a half-filled band, in agreement with the chemical composition of dimerized systems.

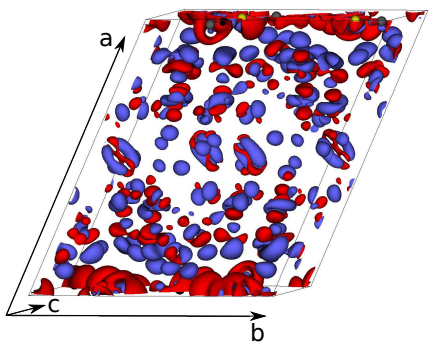

Figure S8: DFT cation-anion interaction-induced charge distribution of κ-(BEDT-TTF)$_2$Cu$_2$(CN)$_3$: the BEDT-TTF molecules (regions marked in blue) donate electrons via hydrogen bonds to the acceptor anion layers (regions marked in red).

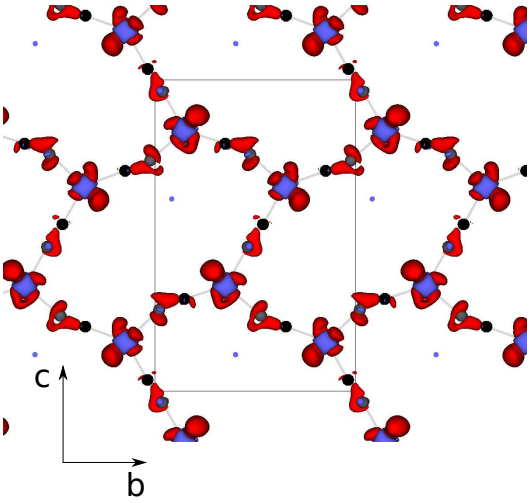

Figure S9: DFT cation-anion interaction-induced charge distribution of the $Cu_2(CN)_3^-$ anion layer in the bc plane. The electron density is enhanced (regions marked in red) at cyanide sites, much more along the chain b-axis than along the bridging c-axis. The largest electron density is concentrated in the vicinity of Cu sites; its distribution differs at Cu sites with two distinct triangular coordination which interchange along the chains in the b direction: Cu atom coordinated with two N atoms and one C atom, or Cu atom coordinated with two C atoms and one N atom.

[S1] M. Dressel and G. Grüner, *Electrodynamics of Solids* (Cambridge University Press, Cambridge, 2002).
[S2] B. P. Gorshunov, A. Volkov, I. E. Spektor, A. S. Prokhorov, A. A. Mukhin, M. Dressel, S. Uchida, and A. Loidl, Int. J. Infrared Millimeter Waves **26**, 1217 (2005).
[S3] M. Dion, H. Rydber, E. Schröder, D. C. Langreth, and B. I. Lundqvist, Phys. Rev. Lett. **92**, 246401 (2004).

[S4] G. Román-Pérez and J. M. Soler, Phys. Rev. Lett. **103**, 096102 (2009).
[S5] J. Klimeš, D. R. Bowler, and A. Michaelides, Phys. Rev. B **83**, 195131 (2011).
[S6] F. Mittendorfer, A. Garhofer, J. Redinger, J. Klimeš, J. Harl, and G. Kresse, Phys. Rev. B **84** 201401 (2011).
[S7] H. J. Monkhorst and J. D. Pack, Phys. Rev. B **13**, 5188 (1976).
[S8] M. Dressel and N. Drichko, Chem. Rev. **104**, 5689 (2004).
[S9] D. Faltermeier, J. Barz, M. Dumm, M. Dressel, N. Drichko, B. Petrov, V. Semkin, R. Vlasova, C. Mézière, and P. Batail, Phys. Rev. B **76**, 165113 (2007); J. Merino, M. Dumm, N. Drichko, M. Dressel, and R.H. McKenzie, Phys. Rev. Lett. **100**, 086404 (2008); M. Dumm, D. Faltermeier, N. Drichko, M. Dressel, C. Mézière, and P. Batail, Phys. Rev. B **79**, 195106 (2009).
[S10] J. Ferber, K. Foyevtsova, H. O. Jeschke, and R. Valentí, Phys. Rev. B **89**, 205106 (2014).

Table S II: Vibrational modes of κ-(BEDT-TTF)$_2$Cu$_2$(CN)$_3$ in the far- and mid-infrared spectral range up to frequencies of approximately 100 THz obtained by *ab-initio* phonon calculations based on density-functional-theory (DFT). C1B0 indicates the lowest-energy configuration with parallel cyanides as shown in Fig. 4 of the main paper, while C2B0 refers to the configuration with reversed c_2 cyanide which is higher in energy by 15 meV.

number	C1B0 Frequency (THz)	C1B0 Frequency (cm^{-1})	C2B0 Frequency (THz)	C2B0 Frequency (cm^{-1})	comments
1	(-0.004)	0	(-0.012)	0	error of calculation yields negative energies close to zero
2	(-0.003)	0	(-0.003)	0	
3	(-0.002)	0	(-0.001)	0	
4	0.729	24.32	0.731	24.38	*b*-axis shear and rocking motion of anion layer; BEDT-TTF motion in the *ac* plane in phase within dimer; gliding of dimers along their extended axes with respect to each other
5	0.998	33.28	0.995	33.19	*c*-axis shear movement of anion layer with respect to BEDT-TTF; breathing BEDT-TTF motion in counterphase to each other within dimer; twisting in-phase motion of BEDT-TTF dimers
6	1.022	34.09	1.026	34.22	out-of-plane vibration of anions; tilting of dimers in-phase oscillation of BEDT-TTF
7	1.054	35.16	1.062	35.42	out-of-plane vibration of anions; wagging of ethylene groups
8	1.134	37.81	1.143	38.14	waving of anion layer along *c*-axis; breathing BEDT-TTF motion in counterphase to each other within dimer; twisting in-phase motion of BEDT-TTF dimers; flipping of ethylene groups
9	1.146	38.23	1.158	38.63	*b*-axis shear movement of anion layer with respect to BEDT-TTF, bending in-phase motion of BEDT-TTF dimers
10	1.155	38.51	1.170	39.02	weak *a*-axis motion of anions; wagging of ethylene endgroups
11	1.215	40.52	1.205	40.18	*b*-axis shear movement of anion layer with respect to BEDT-TTF, bending in-phase motion of BEDT-TTF dimers
12	1.229	41.00			mainly *a*-axis motion of anions gliding of BEDT-TTF within dimer
			1.238	41.30	*b*-axis shear movement of anion layer with respect to BEDT-TTF, bending in-phase motion of BEDT-TTF dimers
13	1.267	42.26	1.273	42.45	waving of anion layer; tilting of BEDT-TTF
14	1.380	46.03	1.380	46.03	sheer motion of coupled BEDDT-TTF and anions
15	1.440	48.04	1.438	47.97	strong out-of-plane motion of anions coupled to BEDT-TTF
16	1.463	48.81	1.466	48.90	*b*-axis motion of anion layer, tilting of bridging CN c_1; rocking of BEDT-TTF dimers
17	1.514	50.51	1.525	50.87	wagging of BEDT-TTF, *c*-axis motion of anions
18	1.549	51.68	1.554	51.83	wagging of BEDT-TTF, *b*-axis motion of anions
19	1.606	53.58	1.596	53.24	gliding of BEDT-TTF, *a*-axis motion of anions
20	1.629	54.32	1.634	54.51	tilting and wagging of BEDT-TTF, *b*-axis motion of anions
21	1.641	54.74	1.645	54.88	torsion motion of BEDT-TTF, *b*-axis motion of anions
22	1.683	56.13	1.689	56.32	vibration of BEDT-TTF, *c*-axis motion of anions
23	1.746	58.24	1.753	58.46	coupled out-of-plane anion motion and BEDT-TTF vibration
24	1.753	58.48	1.755	58.54	
25	1.786	59.59	1.781	59.41	
26	1.853	61.80	1.844	61.51	mainly *c*-axis vibration of anions coupled to BEDT-TTF vibration
27	1.941	64.76	1.955	65.20	27-40: Coupled anion motion with BEDT-TTF vibration; wagging of ethylene endgroups; wagging of Cu bonds, bending of cyanide links
28	2.000	66.70	1.997	66.61	
29	2.040	68.06	2.039	68.00	
30	2.090	69.72	2.092	69.77	
31	2.122	70.77	2.127	70.96	
32	2.157	71.96	2.167	72.29	
33	2.164	72.18	2.169	73.34	
34	2.280	76.05	2.288	76.32	

Table S II: Continued

number	C1B0 Frequency (THz)	C1B0 Frequency (cm^{-1})	C2B0 Frequency (THz)	C2B0 Frequency (cm^{-1})	comments
35	2.290	76.39	2.295	76.56	
36	2.333	77.80	2.338	77.99	
37	2.435	81.21	2.442	81.45	
38	2.474	82.51	2.483	82.82	
39	2.484	82.85	2.493	83.15	
40	2.539	84.69	2.545	84.89	
41	2.555	85.21	2.561	85.43	41-62: rotation of Cu bonds and twisting of cyano bonds; rocking of ethylene groups
42	2.566	85.59	2.573	85.81	
43	2.594	86.52	2.600	86.72	
44	2.630	87.71	2.641	88.10	
45	2.727	90.96	2.727	90.97	
46	2.748	91.68	2.752	91.79	
47	2.853	95.18	2.857	95.28	
48	2.883	96.18	2.892	96.47	
49	2.969	99.04	2.965	98.89	
50	2.976	99.25	2.996	99.95	
51	3.030	101.06	3.039	101.37	
52	3.044	101.54	3.052	101.81	
53	3.055	101.91	3.071	102.43	
54	3.119	104.02	3.125	104.25	
55	3.271	109.10	3.281	109.46	
56	3.306	110.27	3.311	110.43	
57	3.446	114.95	3.470	115.74	
58	3.490	116.40	3.486	116.29	
59	3.653	121.85	3.649	121.70	
60	3.714	123.89	3.716	123.97	
61	3.720	124.78	3.741	124.80	
62	3.757	125.32	3.744	124.88	
63	3.858	128.70	3.873	129.78	63-68: bending and stretching of anions coupled to BEDT-TTF
64	3.870	129.08	3.873	129.20	
65	3.967	132.34	3.977	132.66	
66	3.981	132.80	3.985	132.94	
67	3.992	133.15	4.001	133.47	
68	4.009	133.72	4.020	134.10	
69	4.050	135.09	4.054	135.22	twist of cyanides, rotation motion of Cu coupled to BEDT-TTF
70	4.154	138.57	4.182	139.49	out-of-plane bending of cyanides, mainly c_1 and c_2, coupled to BEDT-TTF
71	4.280	142.77	4.283	142.88	out-of-plane bending of cyanides, mainly b_3 and b_4; coupled to BEDT-TTF
72	4.306	143.63	4.350	145.09	out-of-plane bending of cyanides coupled to BEDT-TTF
73	4.755	158.60	4.702	156.84	73-78: anion motion coupled to BEDT-TTF; bending and stretching of cyanides; mainly *c*-direction
74	4.836	161.32	4.760	158.76	
75	4.848	161.70	4.850	161.76	
76	4.950	165.11	4.945	164.93	
77	4.983	166.22	4.976	165.99	
78	5.065	168.96	5.015	167.28	78-83: anion motion coupled to BEDT-TTF; bending and stretching of cyanides
79	5.159	172.09	5.227	174.34	
80	5.407	180.36	5.411	180.50	80-83: anion motion coupled to twisting BEDT-TTF; bending and stretching of cyanides
81	5.414	180.60	5.414	180.59	
82	5.491	183.20	5.495	183.30	
83	5.504	183.59	5.505	183.63	

Table S II: Continued

number	C1B0 Frequency (THz)	C1B0 Frequency (cm^{-1})	C2B0 Frequency (THz)	C2B0 Frequency (cm^{-1})	comment
84	5.844	194.94	5.894	196.61	84-88: twisting and stretching anion layer coupled to ethylene endgroups
85	5.963	198.91	6.016	200.68	
86	6.177	206.05	6.020	200.80	
87	6.455	215.32	6.536	218.00	
88	6.741	224.86	6.774	225.96	
89	6.916	230.69	6.921	230.86	89-96: bending of BEDT-TTF; no anion motion
90	6.946	231.69	6.951	231.87	
91	7.257	242.06	7.263	242.28	
92	7.263	242.26	7.276	242.69	
93	7.302	243.59	7.310	243.82	
94	7.313	243.92	7.325	244.34	
95	7.422	247.56	7.436	248.03	
96	7.440	248.16	7.455	248.66	
97	7.636	254.72	7.641	254.86	97-104: wagging movement of BEDT-TTF coupled to-out-plane motion of anions
98	7.661	255.54	7.644	254.97	
99	7.699	256.81	7.701	256.87	
100	7.730	257.84	7.729	257.80	
101	7.774	259.30	7.781	259.56	
102	7.791	259.87	7.798	260.12	
103	7.867	262.40	7.843	261.62	
104	7.883	262.95	7.885	263.02	
105	7.984	266.31	7.947	265.07	105-106: out of plane twist of cyanides, coupled to BEDT-TTF vibration mainly c_1 and b_2
106	8.029	266.31	7.968	265.77	mainly c_2 and b_4
107	8.089	269.81	8.093	269.96	107-114: rocking of ethylene endgroups coupled to anions
108	8.103	270.29	8.112	270.60	
109	8.157	272.09	8.128	271.12	
110	8.210	273.84	8.201	273.55	
111	8.392	279.73	8.408	280.46	
112	8.400	280.21	8.416	280.74	
113	8.443	281.63	8.458	282.13	
114	8.485	283.04	8.494	283.32	
115	8.769	292.49	8.703	290.31	115-120: twisting of cyanides coupled to rocking ethylene groups
116	8.799	293.51	8.783	292.96	
117	8.836	294.74	8.835	294.72	
118	8.897	296.76	8.895	296.79	
119	8.939	298.17	8.937	298.11	
120	9.026	301.07	8.956	298.73	

Table S II: Continued

number	C1B0 Frequency (THz)	C1B0 Frequency (cm^{-1})	C2B0 Frequency (THz)	C2B0 Frequency (cm^{-1})	comment
121	9.280	309.56	9.282	309.61	121-125: various BEDT-TTF vibrations coupled with anion vibrations
122	9.286	309.75	9.286	309.75	
123	9.309	310.52	9.314	310.69	123-129: twisting of cyanides
124	9.361	312.26	9.328	311.16	
125	9.390	313.23	9.389	313.17	125-129: twisting of cyanides coupled with weak rocking of ethylene endgroups
126	9.496	316.74	9.589	319.27	mainly b_3 and b_1, and c_1 and c_2
127	9.635	321.38	9.746	325.09	
128	9.883	329.66	9.823	327.66	mainly b_4 and b_2, and c_1 and c_2
129	10.190	339.89	10.037	334.80	additional BEDT-TTF tilting
130	10.293	343.35	10.184	339.69	130-144: twisting and shuffling of BEDT-TTF coupled with anion vibrations; rocking of ethylene endgroups
131	10.320	344.25	10.288	343.16	
132	10.338	344.84	10.316	343.16	
133	10.356	345.45	10.338	344.83	
134	10.382	346.30	10.356	345.43	134-144: twisting of cyanides
135	10.418	347.49	10.381	346.26	
136	10.420	347.57	10.392	346.64	
137	10.427	347.80	10.427	347.80	
138	10.485	349.73	10.428	347.85	
139	10.520	350.90	10.511	350.60	
140	10.562	352.30	10.550	351.92	
141	10.583	353.03	10.566	352.44	
142	10.602	353.66	10.595	353.42	
143	10.703	357.03	10.673	356.00	143-144: strong twisting of cyanides
144	11.211	373.95	11.301	376.96	
145	11.684	389.72	11.674	389.42	145-148: antisymmetric breathing modes of BEDT-TTF rings
146	11.696	390.13	11.687	389.83	
147	11.729	391.25	11.720	390.94	
148	11.743	391.72	11.734	391.42	
149	12.982	433.04	12.969	432.60	149-160: symmetric breathing modes of BEDT-TTF rings
150	13.016	434.18	13.005	433.79	
151	13.021	434.32	13.007	433.88	
152	13.046	435.16	13.034	434.75	
153	13.572	452.73	13.564	452.45	
154	13.582	453.05	13.574	452.79	
155	13.619	454.29	13.614	454.11	
156	13.624	454.46	13.616	454.18	
157	13.661	455.69	13.651	455.36	
158	13.676	456.17	13.669	455.96	
159	13.746	458.52	13.737	458.23	
160	13.749	458.61	13.739	458.27	

Table S II: Continued

number	C1B0 Frequency (THz)	C1B0 Frequency (cm^{-1})	C2B0 Frequency (THz)	C2B0 Frequency (cm^{-1})	comment
161	13.762	459.04	13.758	458.91	161-170: symmetric breathing modes of BEDT-TTF rings
162	13.780	459.64	13.767	459.23	
163	13.800	460.30	13.773	459.43	
164	13.828	461.24	13.803	460.43	
165	13.844	461.78	13.836	461.51	
166	13.921	464.36	13.916	464.20	
167	13.978	466.27	13.974	466.11	
168	13.997	466.89	13.991	466.68	breathing of inner rings; dimers in phase
169	14.085	469.82	14.077	469.57	breathing of inner rings in all four BEDT-TTF
170	14.215	474.46	14.140	471.64	vibration of cyanide group as a whole, mainly b_4 and b_2 coupled with weak rocking of ethylene endgroups
171	14.278	476.27	14.269	475.98	171-172: antisymmetric breathing of inner rings within dimer; rocking of central C=C
172	14.284	476.45	14.275	476.16	
173	14.346	478.52	14.338	478.25	173-174: symmetric breathing of inner rings within dimer; rocking of central C=C
174	14.478	482.94	14.416	480.87	coupled with anion vibrations
175	14.506	483.88	14.472	482.74	175-180: Cu-CN-Cu motion; rocking of outer C=C bonds of BEDT-TTF; dominant motion of b_3 and also b_4; dominant rocking of one outer C=C
176	14.590	485.66	14.552	485.39	dominant motion of b_1 and also b_2
177	14.577	486.23	14.560	485.67	
178	14.589	486.64	14.571	486.05	
179	14.595	486.83	14.575	486.17	dominant motion of b_1 and b_4
180	14.604	487.15	14.649	488.63	dominant motion of b_1 and b_2
181	14.667	489.24	14.650	488.68	181-184: tilting motion of one outer C=C bond and outer ring of BEDT-TTF
182	14.670	489.34	14.656	488.86	
183	14.672	489.40	14.657	488.90	
184	14.675	489.45	14.807	493.92	
185	15.215	507.51	15.243	508.46	185-186: vibration of cyanides with respect copper ions: Cu-CN-Cu; c_1 and c_2 are in phase
186	15.402	513.74	15.447	515.26	c_1 and c_2 are out of phase
187	17.997	600.32	17.997	600.31	187-200: rocking of ethylene endgroups
188	18.000	600.42	18.000	600.41	
189	18.010	600.75	18.014	600.88	
190	18.015	600.91	18.017	600.99	
191	18.206	607.29	18.201	607.11	
192	18.208	607.35	18.203	607.17	
193	18.230	608.09	18.212	607.50	
194	18.235	608.27	18.214	607.54	
195	19.128	638.05	19.128	638.03	
196	19.133	638.19	19.133	638.22	
197	19.148	638.71	19.149	638.75	
198	19.149	638.74	19.153	638.87	
199	19.222	641.16	19.218	641.03	
200	19.227	641.35	19.221	641.15	

Table S II: Continued

number	C1B0 Frequency (THz)	C1B0 Frequency (cm^{-1})	C2B0 Frequency (THz)	C2B0 Frequency (cm^{-1})	comment
201	19.231	641.49	19.223	641.19	201-202: rocking of ethylene endgroups
202	19.242	641.84	19.225	641.29	
203	22.346	745.38	22.327	744.76	203-210: rocking of C-C and ethylene endgroups; twist of outer ring of BEDT-TTF
204	22.369	746.14	22.351	745.55	
205	22.385	746.69	22.366	746.06	
206	22.396	747.04	22.377	746.43	
207	22.517	751.09	22.491	750.21	twist of outer ring at one BEDT-TTF side
208	22.523	751.30	22.504	750.65	
209	22.529	751.50	22.506	750.73	
210	22.556	752.40	22.535	751.68	
211	22.720	757.87	22.718	757.79	211-214: longitudinal translation of central C=C bond of BEDT-TTF; rocking of ethylene endgroups
212	22.730	758.18	22.728	758.13	
213	22.743	758.64	22.739	758.48	
214	22.749	758.84	22.745	758.68	
215	24.939	831.87	24.940	831.90	214-218: transverse translation of central C=C bond of BEDT-TT; rocking of ethylene endgroups
216	24.945	832.08	24.947	832.13	
217	24.970	832.91	24.969	832.87	
218	24.984	833.35	24.983	833.34	
219	25.112	837.63	25.072	836.32	219-222: symmetric translations of outer C=C and breathing of rings; rocking of ethylene endgroups
220	25.141	838.60	25.102	837.32	
221	25.149	838.89	25.108	837.52	
222	25.191	840.28	25.150	838.90	
223	25.327	844.81	25.289	843.54	223-226: asymmetric translations of outer C=C and breathing of inner rings; rocking of ethylene endgroups
224	25.379	846.57	25.343	845.34	
225	25.392	846.97	25.354	845.71	
226	25.406	847.46	25.369	846.22	
227	25.931	864.96	25.929	864.90	227-240 rocking of ethylene endgroups
228	25.954	865.74	25.949	865.57	
229	25.959	865.91	25.960	865.94	
230	25.978	866.53	25.973	866.39	
231	26.182	873.34	26.171	872.98	
232	26.190	873.62	26.174	873.07	
233	26.202	873.99	26.196	873.81	
234	26.226	874.82	26.218	874.54	
235	27.086	903.51	27.076	903.16	
236	27.096	903.84	27.085	903.46	
237	27.108	903.84	27.103	904.07	
238	27.109	904.26	27.104	904.08	
239	27.199	907.27	27.174	906.42	
240	27.214	907.76	27.188	906.91	

Table S II: Continued

number	C1B0 Frequency (THz)	C1B0 Frequency (cm^{-1})	C2B0 Frequency (THz)	C2B0 Frequency (cm^{-1})	comment
241	27.237	908.52	27.212	907.69	241-242: rocking of ethylene endgroups
242	27.254	909.09	27.228	908.24	
243	28.552	952.38	28.500	950.66	243-262: twist of C=C bonds of BEDT-TTF
244	28.566	952.85	28.514	951.11	
245	28.593	953.75	28.540	952.01	
246	28.605	954.15	28.551	952.35	
247	28.722	958.07	28.669	956.30	
248	28.742	958.72	28.689	956.95	
249	28.781	960.02	28.730	958.32	
250	28.801	960.70	28.750	958.99	
251	29.238	975.27	29.205	974.19	
252	29.240	975.35	29.212	974.39	
253	29.256	975.89	29.220	974.68	
254	29.261	976.04	29.229	974.98	
255	29.363	979.46	29.345	978.83	strong twist of central C=C bonds
256	29.383	980.11	29.360	979.36	
257	29.398	980.61	29.378	979.93	
258	29.412	981.09	29.381	980.05	
259	29.532	985.08	29.455	982.50	
260	29.538	985.27	29.454	982.51	
261	29.547	985.58	29.465	982.84	
262	29.554	985.83	29.478	983.27	
263	33.235	1108.60	33.233	1108.53	263-270: ethylene endgroups tilting modes
264	33.239	1108.74	33.239	1108.74	
265	33.249	1109.05	33.243	1108.87	
266	33.251	1109.12	33.246	1108.97	
267	33.408	1114.39	33.387	1113.67	
268	33.420	1114.76	33.395	1113.93	
269	33.427	1117.99	33.404	1114.23	
270	33.438	1115.39	33.413	1114.54	
271	34.878	1163.40	34.881	1163.51	271-280: ethylene endgroups wagging modes
272	34.892	1163.88	34.895	1163.96	
273	34.913	1164.60	34.906	1164.35	
274	34.930	1165.15	34.919	1164.78	
275	35.051	1169.17	34.997	1167.39	
276	35.060	1169.48	35.013	1167.91	
277	35.068	1169.75	35.021	1168.18	
278	35.090	1170.49	35.048	1169.07	
279	37.592	1253.93	37.586	1253.72	
280	37.601	1254.23	37.602	1254.28	

Table S II: Continued

number	C1B0 Frequency (THz)	C1B0 Frequency (cm^{-1})	C2B0 Frequency (THz)	C2B0 Frequency (cm^{-1})	comment
281	37.615	1254.70	37.605	1254.37	281-294: ethylene endgroups wagging modes
282	37.621	1254.59	37.610	1254.53	
283	37.669	1256.49	37.634	1255.35	
284	37.681	1256.89	37.637	1255.44	
285	37.706	1257.23	37.679	1256.85	
286	37.722	1258.26	37.685	1257.06	
287	38.153	1272.66	38.151	1272.59	
288	38.170	1273.21	38.166	1273.08	
289	38.178	1273.47	38.177	1273.45	
290	38.198	1274.14	38.195	1274.06	
291	38.611	1287.92	38.614	1288.04	
292	38.633	1288.67	38.617	1288.14	
293	38.639	1288.86	38.640	1288.90	
294	38.665	1289.71	38.651	1289.27	
295	41.479	1383.58	41.583	1387.06	295-297: symmetric C=C vibrations; $\nu_3(a_g)$ in D_{2h} molecular symmmetry; two dimers are out of phase
296	41.489	1383.92	41.594	1387.43	
297	41.673	1390.05	41.774	1393.45	
298	42.346	1412.50	42.340	1412.30	298-318: ethylene endgroups scissoring modes
299	42.383	1413.75	42.370	1413.30	
300	42.383	1413.76	42.379	1413.62	
301	42.393	1414.08	42.380	1413.66	
302	42.535	1418.81	42.509	1417.93	
303	42.560	1419.64	42.533	1418.74	
304	42.591	1420.68	42.573	1420.07	
305	42.594	1420.79	42.583	1420.40	
306	42.604	1421.11	42.590	1420.45	
307	42.614	1421.43	42.610	1421.32	
308	42.621	1421.69	42.620	1421.63	
309	42.633	1422.07	42.627	1421.88	
310	42.748	1425.91	42.847	1429.22	antisymmetric C=C vibrations; $\nu_{27}(b_{1u})$ in D_{2h} molecular symmmetry; out of phase within dimer; two dimers are in-phase
311	42.826	1428.54	42.928	1431.92	antisymmetric C=C vibrations; $\nu_{27}(b_{1u})$ in D_{2h} molecular symmmetry; out of phase within dimer; two dimers are out-of-phase
312	42.898	1430.91	42.960	1433.00	antisymmetric C=C vibrations; $\nu_{27}(b_{1u})$ in D_{2h} molecular symmmetry; in-phase within dimer; two dimers are out-of-phase
313	42.927	1431.89	42.974	1433.45	antisymmetric C=C vibrations; $\nu_{27}(b_{1u})$ in D_{2h} molecular symmmetry; all four BEDT-TTF molecules area in phase
314	43.036	1435.54	43.047	1435.88	
315	43.063	1436.43	43.067	1436.57	
316	43.085	1437.15	43.083	1437.10	
317	43.089	1437.30	43.113	1438.10	
318	43.120	1438.32	43.181	1440.35	
319	43.989	1467.30	44.083	1470.45	319-320: symmetric C=C vibrations: ν_2 in D_{2h} molecular symmetry; out of phase within dimers
320	44.000	1467.67	44.094	1470.83	two dimers are out-of-phase

Table S II: Continued

number	C1B0 Frequency (THz)	C1B0 Frequency (cm^{-1})	C2B0 Frequency (THz)	C2B0 Frequency (cm^{-1})	comment
321	44.007	1467.92	44.104	1471.14	symmetric C=C vibrations: ν_2 in D_{2h} molecular symmetry; in phase within dimers, the two dimers are out of phase
322	44.022	1468.43	44.119	1471.66	symmetric C=C vibrations: ν_2 in D_{2h} molecular symmetry; all four BEDT-TTF molecules area in phase
323	62.652	2089.86			cyanide stretching, mainly b_4
			62.895	2097.94	strongest motion in b_4 and b_4
324	62.812	2095.17			cyanide stretching, mainly b_1
			62.947	2099.68	strongest motion in b_1 and b_2
325	63.003	2101.57			cyanide stretching, strongest motion in b_2
			63.012	2101.84	equally strong motion in all four b-type cyanides
326	63.160	2106.78			cyanide stretching, strongest motion in b_3
			63.131	2105.84	equally strong motion in all four b-type cyanides
327	63.910	2131.81	63.940	2132.82	cyanide stretching, out-of-phase vibration of c_1 and c_2
328	64.037	2136.06	64.083	2137.57	cyanide stretching, in-phase vibration of c_1 and c_2
329	89.275	2977.91	89.256	2977.26	329-344: symmetric C-H stretching vibrations in ethylene endgroups
330	89.280	2978.04	89.257	2977.28	
331	89.298	2978.67	89.312	2979.12	
332	89.306	2978.93	89.337	2979.96	
333	89.423	2982.84	89.449	2983.69	
334	89.431	2983.08	89.459	2984.97	
335	89.441	2983.44	89.465	2984.22	
336	89.467	2984.28	89.483	2984.84	
337	89.601	2988.76	89.557	2987.28	
338	89.623	2989.51	89.558	2987.34	
339	89.630	2989.72	89.599	2988.71	
340	89.644	2990.20	89.602	2988.80	
341	89.831	2996.44	89.999	3002.04	
342	89.849	2997.04	90.000	3002.09	
343	89.865	2997.58	90.015	3002.56	
344	89.908	2999.01	90.018	3002.66	
345	90.773	3027.87	90.821	3029.46	345-360: antisymmetric C-H stretching vibrations in ethylene endgroups
346	90.782	3028.17	90.834	3029.88	
347	90.794	3028.55	90.836	3029.96	
348	90.821	3029.45	90.855	3030.61	
349	91.079	3038.07	91.037	3036.68	
350	91.097	3038.68	91.042	3036.85	
351	91.125	3039.59	91.071	3037.79	
352	91.132	3039.83	91.087	3038.34	
353	91.222	3042.84	91.238	3043.37	
354	91.250	3043.78	91.241	3043.48	
355	91.255	3043.94	91.272	3044.50	
356	91.261	3044.14	91.277	3044.68	
357	91.888	3065.05	92.040	3070.14	
358	91.891	3065.16	92.057	3070.68	
359	91.893	3065.21	92.065	3070.67	
360	91.917	3066.02	92.066	3070.98	